JSEE Vol. 21, No. 2, 2019 DOI:10.48303/jsee.2019.240813

Experimental and Numerical Investigation of Steel Frame with Shear Panel at Mid-Span

Hadis Mohammad Moradi[1] and Behrokh Hosseini Hashemi[2]*

1. Ph.D. Student, International Institute of Earthquake Engineering and Seismology (IIEES), Tehran, Iran
2. Associate Professor, Structural Engineering Research Center, International Institute of Earthquake Engineering and Seismology (IIEES), Tehran, Iran,
* Corresponding Author; email: behrokh@iiees.ac.ir

Received: 15/09/2019
Accepted: 05/02/2020

ABSTRACT

During the last two decades, the semi-supported steel shear wall (SSSW) has been introduced as an alternative to the traditional form of steel plate shear wall (SPSW) system. In this paper, a numerical and experimental study on the behavior of a pinned connection steel frame with a mid-span shear panel, as well as the effect of opening existence on the system behavior is investigated. In this system, shear panel consisting of infill steel plate, stiffeners perpendicular to infill plate and secondary columns are placed in the middle of the steel frame span with pinned connections and unlike conventional SPSW system and SSSW system, the buckling of the infill plate is prevented and energy dissipation is carried out by shear. Experimental studies were performed on two specimens with a scale of 1:2. The characteristics of both specimens are the same and the only difference is the presence of opening in the second specimen. The results showed that in both specimens, the hysteretic curves were spindle-shape and without pinching. Moreover, numerical results were in good agreement with the experimental ones. Numerical studies showed that the energy dissipation and shear strength were increased with decreasing the opening ratio as well as decreasing height to thickness ratio of the infill plate. For example, in models with slenderness ratio of 200, the dissipated energy and maximum strength in the model with an opening ratio of 0.4 were about 47% and 38% less than that of the model without opening, respectively.

Keywords:
Steel shear panel; Opening ratio; Beam only connected web plates; Hysteretic, Dissipated energy

1. Introduction

The steel plate shear wall system has been used as a lateral load resisting structural system for more than 40 years and many researchers have conducted numerical and experimental studies on this system [1-5]. In the conventional steel shear wall system, the main part of the system strength is provided by the post-buckling strength of the steel plate. Development of the tension field, after the buckling of the infill plate, induces high stress levels in the circumferential columns. Therefore, strong columns should be used to prevent the formation of plastic hinges in the columns [6]. This leads to the use of non-economical sections for columns in steel shear wall structures.

In SPSWs, tension field action applies large stresses on surrounding elements which may lead to early failure of the column [7]. To alleviate this problem, some investigations including the use of cold-formed, light-gauge steel for infill plate [8], the use of low yield strength steel [9], cutting holes throughout the plate in a specified regular pattern [10] and the use of the steel shear wall system in which the infill plate are attached only to the beams, as suggested in [11], have been performed.

In the last two decades, several studies have been carried out on the shear wall system in which infill plates are attached only to the beams [12-13]. Jahanpour et al. [14] performed numerical and experimental studies on SSSW systems. In this system, the connection of infill plate and columns is removed and secondary columns are added to the system. Besides the stresses caused by the extension of the tension field are applied to the beams and secondary columns. Their research results showed that the system, in addition to its considerable shear strength, solved the problem of using large non-economical columns and could be used as an independent seismic load resisting system. The general shape of the hysteretic curves obtained from the experimental results was S-shaped and the occurrence of pinching phenomena was significant. Clayton et al. [15] compared the behavior of conventional SPSWs with that of SPSW systems in which the plate is attached only to beams. The results of their studies showed that removing the connection between infill plates and columns would significantly reduce steel consumption by reducing column demand, especially in tall structures. Shekastehband et al. [7, 16] conducted numerical and experimental studies on the seismic behavior of the shear walls with fully-connected and beam-only-connected web plates. The results of their studies showed that removing the connection of infill plate and columns significantly reduces the energy dissipation and shear strength and increases the ductility. They also examined the effect of four perforation diameters as well as two slenderness ratios of infill plates on the seismic behavior of SSSWs. They found out based on the test results, the strength, stiffness, ductility factor and energy dissipation characteristics of the specimens were substantially reduced in specimens with openings. Moreover, in all of the studied specimens, the pinching effect induced by out-of-plane buckling of the infill plate was observed.

The steel plate shear wall system in which the infill plate is attached only to the beams also has shortcomings, despite the fact that it has solved the main problem of the conventional steel plate shear wall system, i.e. the need for strong and non-economical columns. For example, due to the plate buckling in the early stages of lateral loading, the phenomenon of pinching occurs in hysteretic curves. In this study, by changing the attitude of governing failure mode and energy dissipation mechanism of SSSW system, a shear panel at the middle of steel frame is designed to absorb energy in shear and eliminate pinching effect in hysteretic curves. Numerical and experimental studies are carried out on the seismic behavior of a pinned steel frame system with a shear panel in the middle of the span and the effect of the opening on its behavior.

2. Experimental Study

Experimental studies were performed on two 1:2 scale specimens (Sp-1 and Sp-2) at the laboratory of the International Institute of Earthquake Engineering and Seismology. To predict the behavior of real scale structures, the effect of scaling must be studied.

2.1. Specimen Details

The system studied in this research consists of three parts: main frame, shear panel and two boxes. The shear panel consisting of secondary columns, infill plate and stiffeners perpendicular to the infill plate. Shear panel was attached to the main frame beams by the boxes. Unlike the SSSWs, which uses secondary columns to help extend the tension field, in our proposed system the secondary columns are used to enhance the plastic moment of the cross-section of shear panel and make the shear panel behavior similar to a shear link beam behavior. The purpose of employing the box in the system was to make the shear panel repairable and reduce its length to absorb energy in the shear.

The geometrical properties of the panel were determined based on the shear link beam criteria, $e < 1.6\ Mp/Vp$ [17]. In this system, the secondary columns were considered as beam flanges and the infill plate as beam web. The basis of the system design was on the fact that the energy dissipation of the system be provided by the shear panel, so the beam and column sections were chosen so that they would not enter the plastic area before the shear panel full yielding. The beams are designed for plastic shear capacity of the panel and columns for gravity load as well as the moment transferred from the beam-to-column joints. The spacing of

stiffener perpendicular to the infill plate in shear panel were calculated according to the AISC-341-10 criteria for spacing of web stiffeners in the shear link beam, as Equation (1). [17].

$$30t_w - \frac{d}{5} \qquad \gamma = 0.02 \tag{1}$$

The geometrical and materials properties in the two specimens Sp-1 and Sp-2 are the same, and the only difference in the specimens was the presence of opening in the Sp-2 specimen. In this specimen, three openings were cut on the panel surface with a dimension of 300×80 mm. The beams and columns of the main frame were IPB240 and IPB160, respectively. Beam to column connections and column to base plate connections were considered pinned. For this purpose, the beam web was attached to the column flange with two 200×120×15 mm plates by full penetration welding. At each bearing location, columns web were attached to the base plate by full penetration welding of 250×100×20 mm plates. The thickness of the shear panel infill plate was 6 mm, which was connected to IPB120 secondary columns by full penetration welding. The dimensions of the perpendicular stiffeners were 400×50×10 mm; and their maximum spacing was 115 mm. Figure (1) presents the details of Sp-1 and Sp-2 specimens.

Table (1) shows the dimensions of the two experimental specimens. The tensile coupon tests were conducted according to ASTM-A370 [18]. The material properties obtained by the coupon tests are given in Table (2).

2.2. Test Setup and Instrumentation

Setup components consist of the reaction frame, strong floor, hydraulic actuator, loading beam located above the frame and the test specimen (Figure 2). For horizontal load transfer, a loading beam made of IPB-220 profile was used with

Table 1. Dimensions and section properties of specimens.

Sample	L (mm)	H (mm)	b (mm)	h (mm)	Beam Section	Column Section	Opening Ratio
Sp-1	1860	1390	640	730	IPB240	IPB160	0
Sp-2	1860	1390	640	730	IPB240	IPB160	0.2

Table 2. Mechanical properties of steel materials from tension coupon tests.

Section	Elastic Modulus (Gpa)	Yield Stress fy (Mpa)	Ultimate Stress fu (Mpa)	Yield Strain (%)	Ultimate Strain εu (%)	Rupture Strain (%)
IPB240	200	340	530	0.15	27	41
IPB160	195	330	490	0.17	21	32
IPB120	185	330	460	0.18	18	28
Plate 6 mm	220	300	405	0.16	30	44

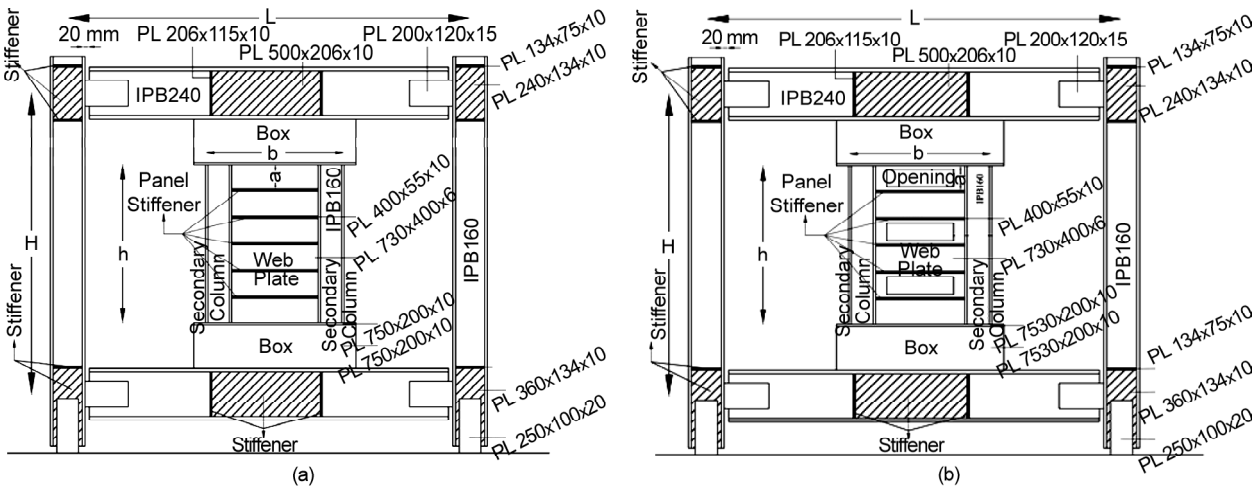

Figure 1. Mechanical properties of steel materials from tension coupon tests.

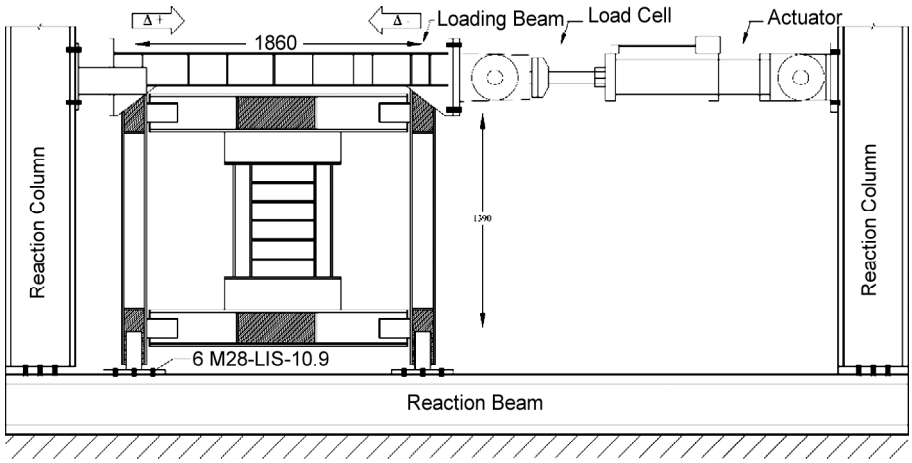

Figure 2. Schematic view of test setup.

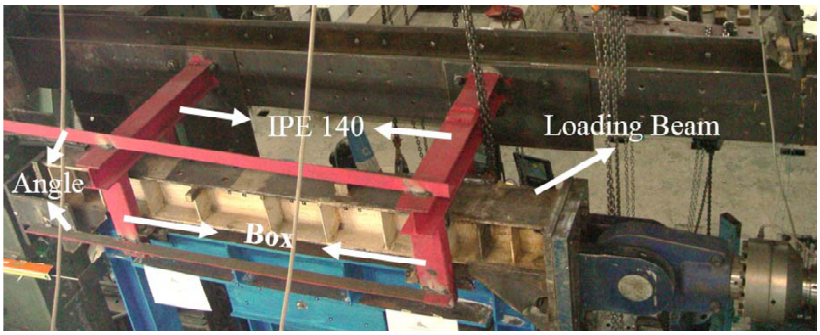

Figure 3. Lateral restrain system of the specimens in the laboratory.

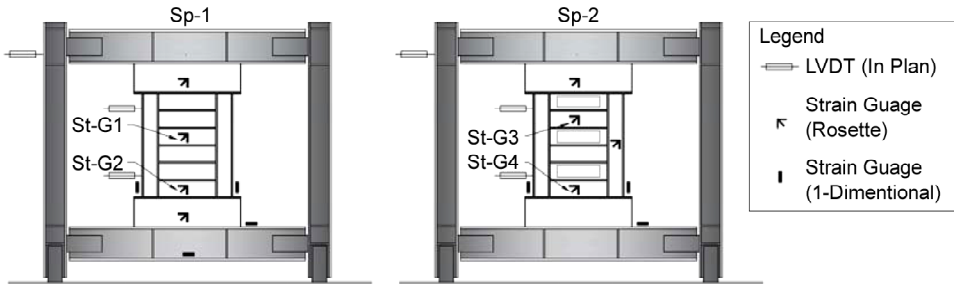

Figure 4. Position of transducers and strain gauges in the Sp-1 and Sp-2 specimens.

stiffeners perpendicular to its web and two plates were welded at the both ends. Six M28-HS-10.9 bolts were used to attach each of the 400×350×30 mm baseplates to the reaction frame. The specimens were tested under a quasi-static cyclic load by means of an actuator of 1000 kN capacity. In order to measure load during the tests, a load cell located between hydraulic jack and loading point was used. To prevent out-of-plane buckling of the frame, the lateral restrain system was designed as shown in Figure (3).

To measure lateral displacement, three linear variable differential transformers (LVDTs) were mounted on each specimen. To measure the strain values at critical locations in the specimens, 15 strain gauges were used: four strain rosettes in each specimen Sp-1 and Sp-2, four uniaxial strain gauges in the Sp-1 specimen and three uniaxial strain gauges in the Sp-2 specimen. Figure (4) shows where the strain gauges were installed.

2.3. Cyclic Loading Protocol

Quasi-static lateral loading was applied to the loading beam in accordance with SAC Protocol [19]. The loading history consists of stepwise increasing deformation cycles as illustrated in Table (3). The deformation parameter used to control the loading history is the interstory drift ratio, defined as interstory displacement divided by story height.

3. Experimental Results

3.1. General Observations

The specimens behaved linearly during the initial displacement. In the Sp-1 specimen, at 1% drift ratio yielding of infill plate occurred on the back of shear panel (Figure 5). In this specimen the test was continued until the drift ratio of 2%, due to the limitations of loading on the reaction column. In the Sp-2 specimen, the test progressed until the drift ratio of 4%. In both specimens, in the 24th cycle (1.5% drift ratio), color cover was peeled off due to yielding in the secondary column webs (Figures 6 and 7).

Continuing the test, in the 25th cycle (2% drift ratio), paint peeling was occurred in the infill plate of shear panel in both specimens, which was due to the extension of the yielding in shear panel (Figures 8 and 9).

In Sp-2, with increasing the drift ratio ratio, yielding of the secondary columns was observed at the flanges bottom. In Figure (10) the deformation and yielding of the secondary column flanges in the 29th cycle (4% drift ratio) is shown.

Figure 3. Loading Protocol based on SAC [19].

Load Step	Drift Ratio (%)	Number of Cycles
1	0.375	6
2	0.5	6
3	0.75	6
4	1	4
5	1.5	2
6	2	2
7	3	2
8	4	2
9	5	2
10	6	2
11	7	2

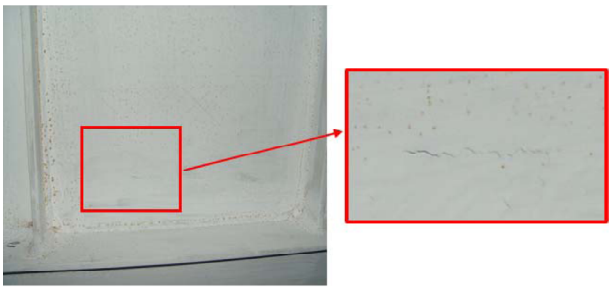

Figure 5. Yielding of infill plate in Sp-1 specimen at 1% drift ratio.

3.2. Strain Gauge Results

The recorded strains versus lateral displacement of the specimens Sp-1 and Sp-2 are presented in Figures (11a) and (11b), respectively. These results are cited as examples for describing the recorded strains. In the St-G1 and St-G2 strain

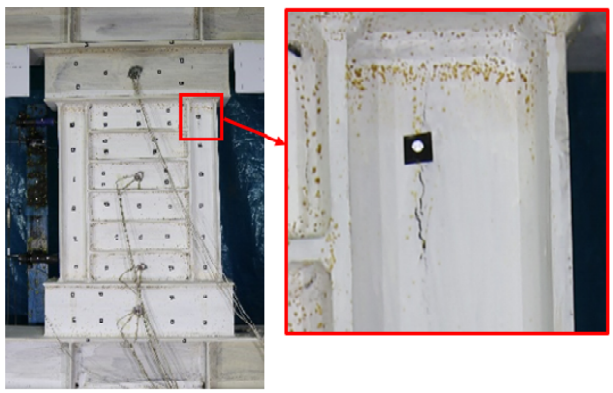

Figure 6. Yielding of the right secondary column web in Sp-1 specimen at 1.5% drift ratio.

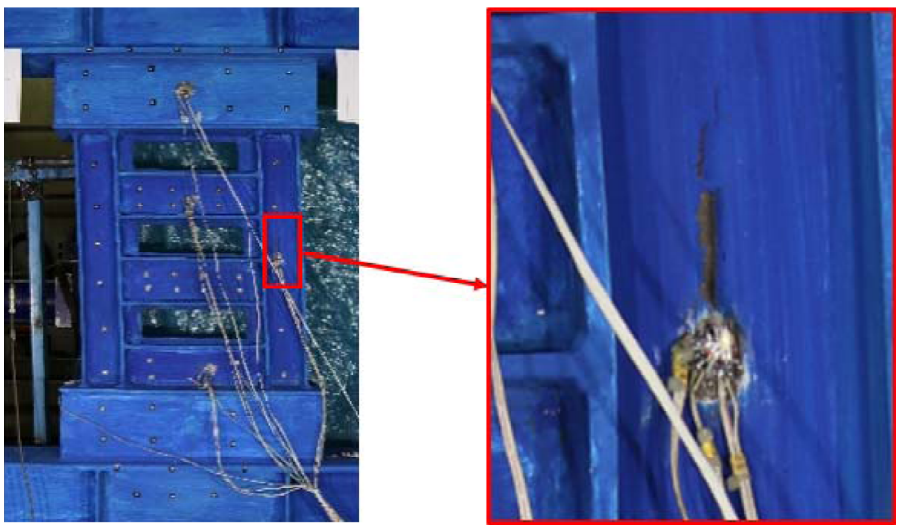

Figure 7. Yielding of the right secondary column web in Sp-2 specimen at 1.5% drift ratio.

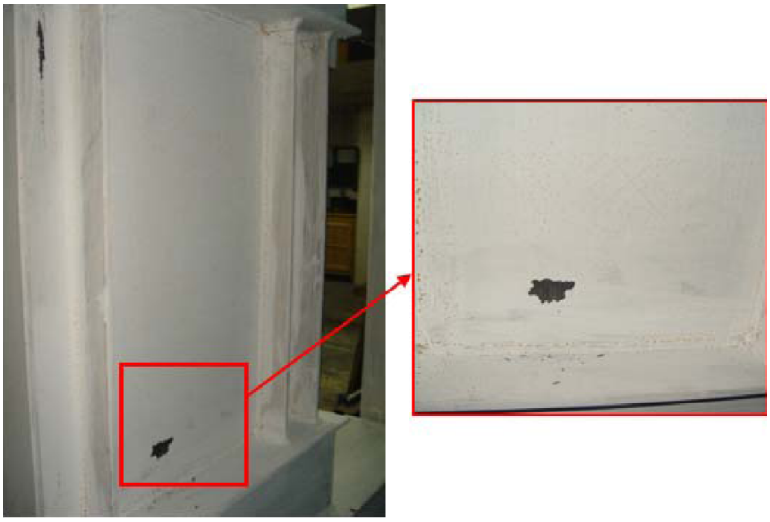

Figure 8. Paint peeling in Sp-1 specimen at 2% drift ratio.

Figure 9. Yielding of infill plate at the back of shear panel in Sp-2 specimen at the 2% drift ratio.

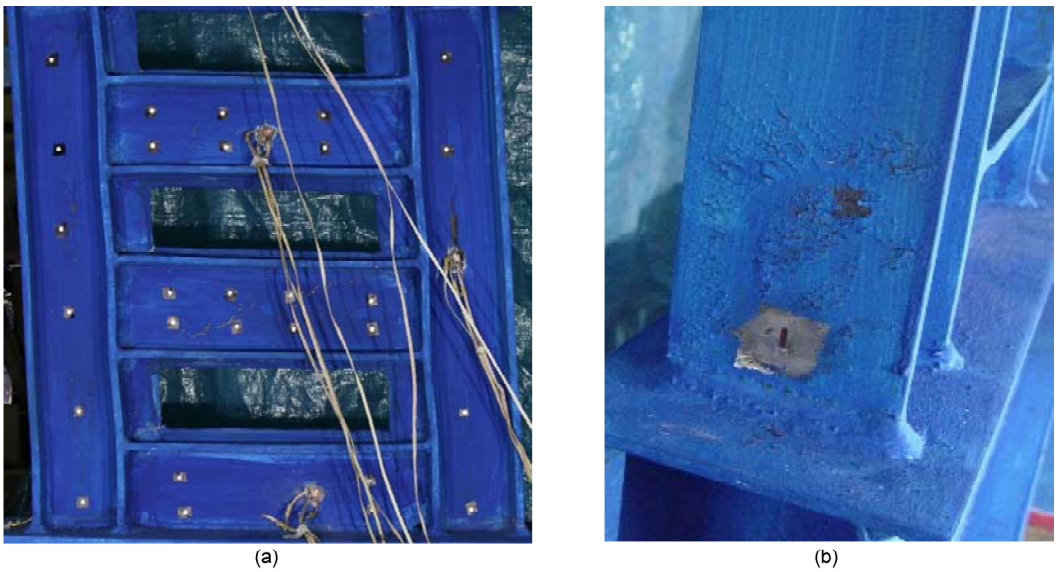

(a) (b)

Figure 10. Yielding in Sp-2 specimen at 4% drift ratio (a) in infill plate (b) at the bottom of secondary column flange.

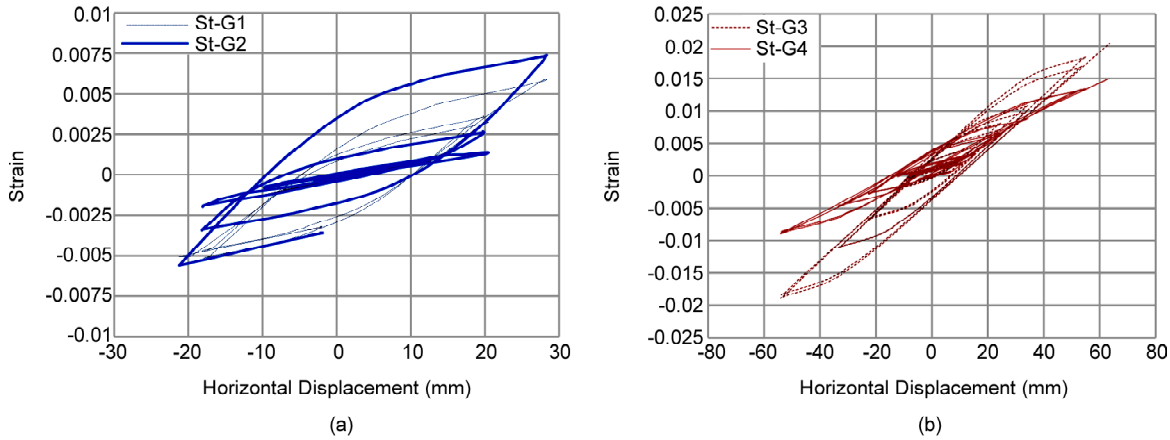

Figure 11. Strain versus lateral displacement: (a) Sp-1; (b) Sp-2.

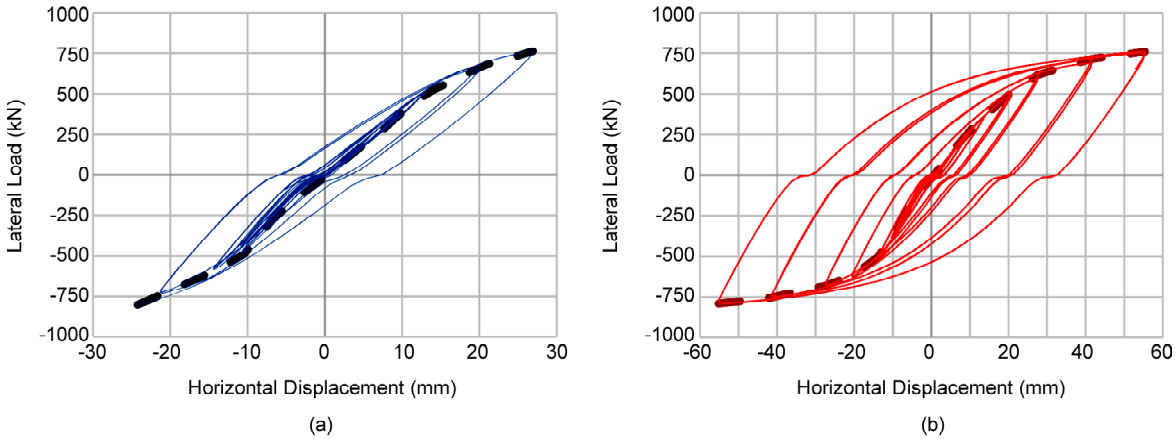

Figure 12. Lateral load versus horizontal displacement curves for (a) Sp-1, (b) Sp-2.

gauges mounted on the Sp-1 infill plate, the envelope strain increased from zero to St-G1=0.0059 and St-G2 = 0.0074, when the specimens were cycled up to 2% drift ratio amplitude. In the Sp-2 specimen, testing continued until drift ratio of 4%. The maximum strain recorded on St-G3 and St-G4 strain gauges mounted on shear panel web plate was 0.02 and 0.015, respectively.

3.3. Hysteretic Behavior of the Specimens

Figure (12) presents the force-displacement hysteretic curves and the back-bone curves for the first and second specimens. Both specimens showed stable hysteretic behavior to the end of loading and the shape of the hysteretic curves of both specimens was spindle-shape. One of the most important advantages of this system is the absence of pinching phenomenon.

Both specimens yielded at 0.5% drift ratio. As the displacement increased, more portions of the infill plate entered the plastic range, causing non-linear inelastic behavior of the system. As mentioned earlier, in the Sp-1 and Sp-2 specimens, testing continued up to cycle 25 (2% drift ratio) and cycle 29 (4% drift ratio) respectively. The presence of opening in the system reduced the elastic stiffness and ultimate shear strength of the system. In the specimen with opening (Sp-2), the elastic stiffness was about 26% lower than that without opening (Sp-1). Moreover, the maximum shear strength of the specimen with opening up to 2% drift ratio was 22% lower than that of the specimen with no openings (Table 4).

Figure (13) shows the comparison of the back-bone curves of the two specimen. As it can be seen, the presence of openings decreased the elastic stiffness and shear strength of the system.

3.4. Stiffness and Energy Dissipation of the Specimens

Secant stiffness is defined as the ratio of the maximum applied load on the specimen, to the

Table 4. The summery result of test specimens.

Specimen	Number of Cycles	Elastic Stiffness K(kN/mm)	K.rel. (kN/mm)/ (kN/mm)	Secant Stiffness at Max Displacement (kN/m)	Max. Strength P_{max} (kN)	Max. Strength at 25th cycle P.25th (kN)	P.25th (kN)/(kN)
Sp-1	25	36.28	1	27.43	762.64	762.64	1
Sp-2	29	26.79	0.74	13.51	751.31	594.16	0.78

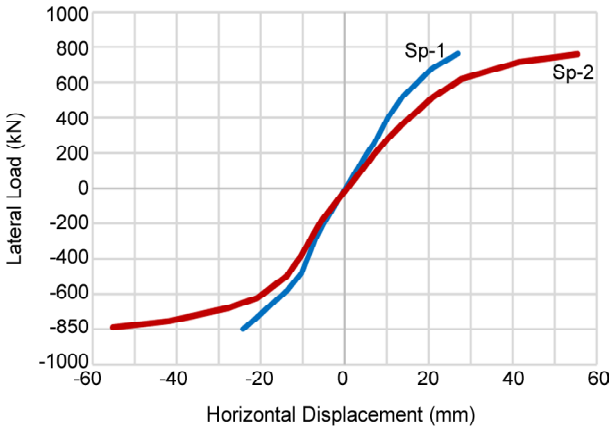

Figure 13. Back-bone of lateral load versus horizontal displacement curves

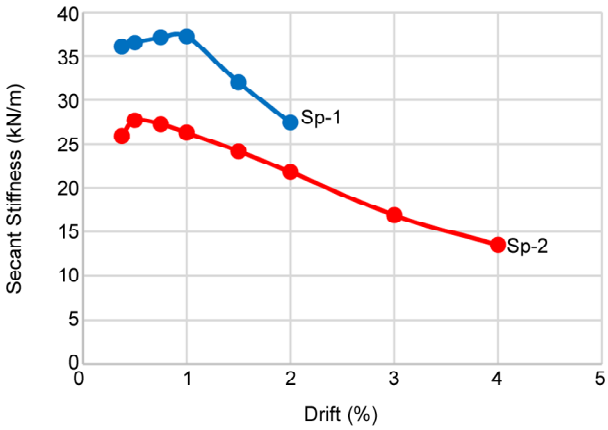

Figure 14. Deterioration of lateral structural stiffness in each drift ratio for specimens Sp-1, Sp-2.

maximum displacement. Figure (14) illustrates the comparison between the secant stiffness versus the drift ratio. As the drift ratio increases, the secant stiffness decreases. The reduction was more rapid in the specimen without opening (Sp-1) than that in the specimen with opening (Sp-2). As can be seen, the secant stiffness of the specimen without opening (Sp-1) was higher than that of the specimen with opening (Sp-2).

Figure (15) shows the dissipated energy versus drift ratio in each specimen. The energy absorbed in each cycle is equal to the area under the hysteretic curve. Given that the first test was stopped at cycle 25th (the first cycle at 2% drift ratio), and the second test at cycle 29th (the first cycle at 4% drift ratio), the dissipated energy-drift ratio diagram in Sp-1 and Sp-2 specimens is shown up to 1.5% and 3% drift ratio, respectively. The amount of dissipated energy until 1% drift ratio was negligible and approximately the same in both specimens. At 1.5% drift ratio, the energy dissipation in the specimen without opening (Sp-1) is about 1.2 times that in the specimen with opening (Sp-2). Moreover, the ratio of cumulative energy loss until 1.5% drift ratio in Sp-1 to Sp-2 was 1.08. The total amount of cumulative energy lost during the test in Sp-1 and Sp-2 specimens was 28.88 kN.m and 148.92 kN.m, respectively.

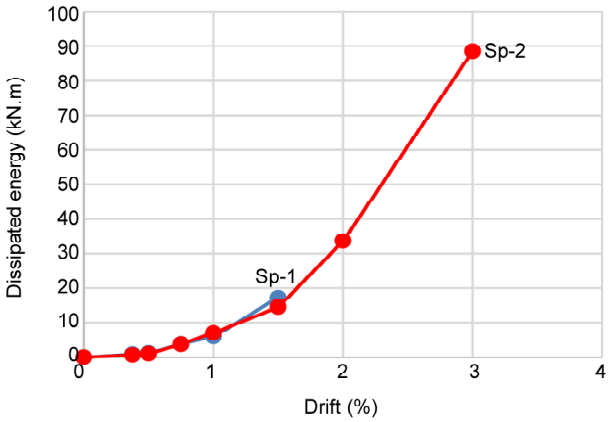

Figure 15. Dissipated energy in each drift ratio for specimens Sp-1, Sp-2.

4. Numerical Analysis

4.1. Finite Element (FE) Modeling

Abaqus FE software [20] was used to analyze the behavior of steel frames with energy absorbing shear panels under cyclic loading. FE analysis can be a suitable method to investigate the behavior of the introduced system and analyze its cyclic behavior. The S4R element was used to mesh all components of the system. After mesh size sensitivity analysis, the largest mesh size of 50mm×50mm was considered. To avoid out-of-plane displacement of frames, the bottom nodes of top beam flanges were restrained from moving out-of-plane. The FE model of the specimen with opening is shown in

Figure (16). The load was applied to the upper beam by increasing the lateral displacement and in accordance with the loading protocol used in the experimental tests. Using the results of the coupon test, the material behavior was modeled as a bilinear model. For the nonlinear behavior of the material, a combined hardening model was considered. This hardening model is a nonlinear combination of Isotropic Hardening and Kinematic Hardening models. The Von Mises yield criterion was used.

Figures (17) and (18) compare the deformation of the two specimens Sp-1 and Sp-2, obtained from numerical and experimental results at 2% and 4% drift ratio, respectively. As can be seen in

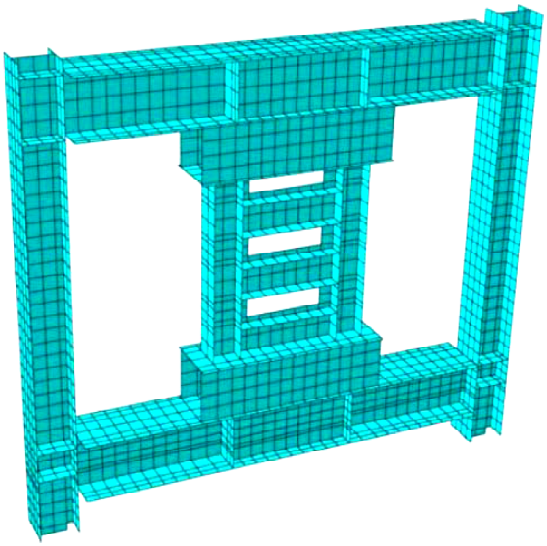

Figure 16. FE model showing of Sp-2.

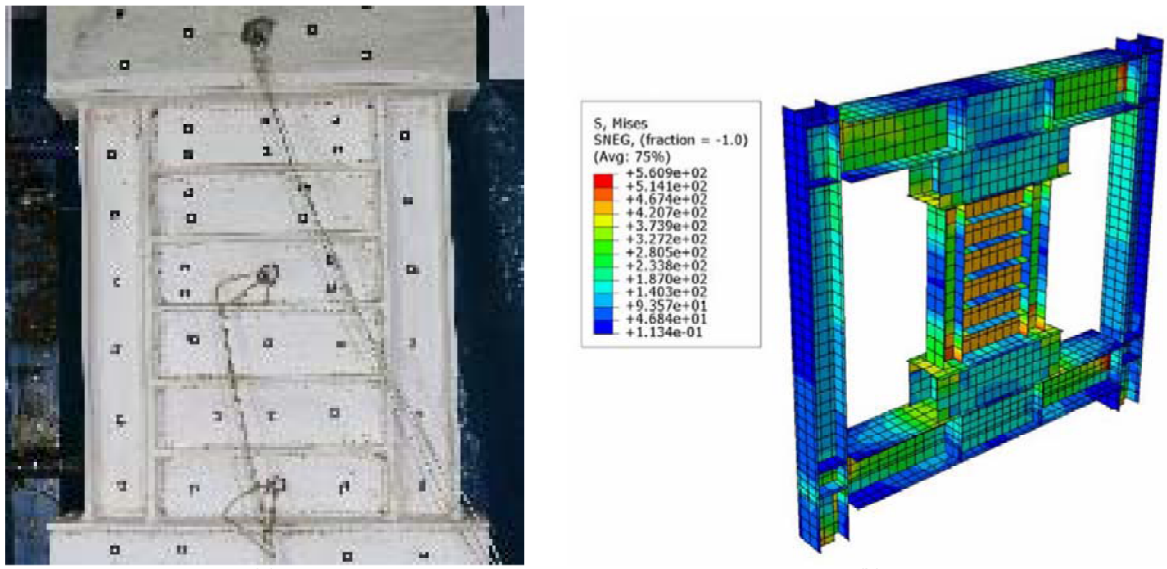

(a) (b)

Figure 17. Deformed shape in Sp-1 at 2% drift ratio (a) Experimental results, (b) Numerical results.

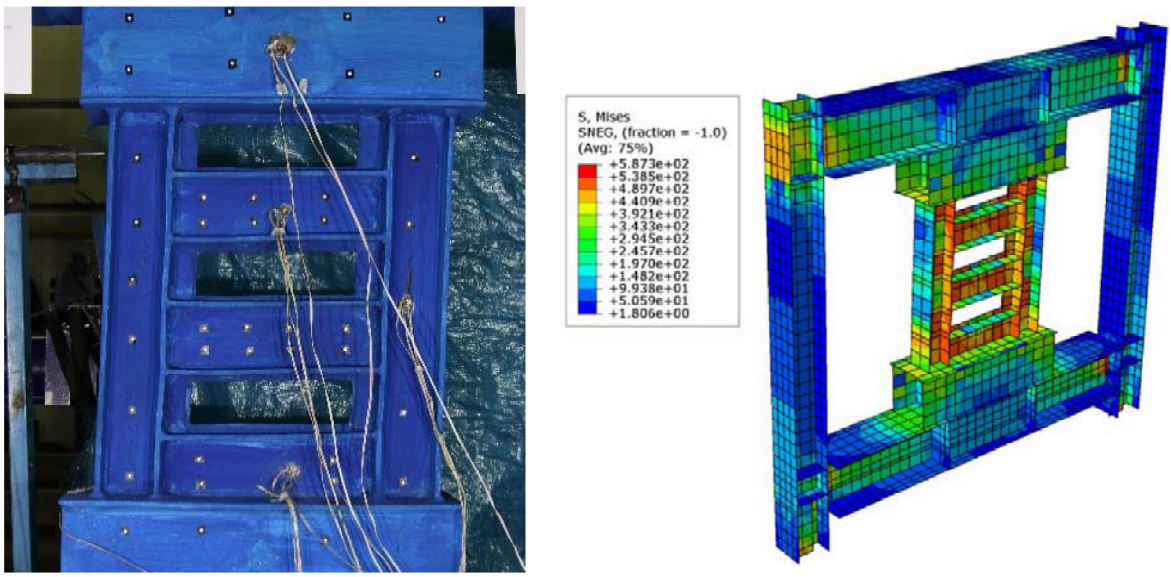

(a) (b)

Figure 18. Deformed shape in Sp-2 at 4% drift ratio (a) Experimental results, (b) Numerical results.

Figures (17a) and (18a), both specimens had shear deformation. Increase in color peel off on the infill plate and secondary column webs during the test resulted from the expansion of the yield surface in the shear panel. Figures (17b) and (18b) show the stress distribution of Von Mises in the two specimens. As expected, all surface of the infill plate of shear panel, as well as the secondary columns were yielded.

Figure (19) shows the comparison of hysteretic and back-bone curves between numerical and experimental results. Pinching effect was not observed in FE analysis, similar to experimental results. The numerical and experimental results are in good agreement with each other. There was a difference between elastic stiffness of the specimens obtained by numerical analysis and that of test results. This difference principally arises as a result of the slippages between loading beam and frame and other localized imperfections that develop upon cyclic loading in the experiments. The FE model can be well used to model the behavior of this system under cyclic load.

In Table (5), the shear capacity obtained from the numerical modeling is compared with the test results. In both specimens, the difference between the shear capacity in the experimental and numerical results is less than 5%.

Figure (20) compares the energy dissipated by each specimen, obtained from the FE analysis and test results, as a function of drift ratio level. As expected, in both specimens, the amount of dissipated energy obtained by numerical analysis was higher than that of obtained from experimental results. In Sp-1 and Sp-2 specimens, at 1.5% drift ratio, the dissipated energy in the FE model was 1.8 and 1.9 times that in the experimental results, respectively. Moreover, in Sp-2, at 3% drift ratio, the energy dissipation calculated by FE model was

Table 5. Comparison of experimental and numerical shear strength.

Specimen	Exp. Shear Strength (kN.m)	Num. Shear Strength (kN.m)	Exp. and Num. Error (%)
Sp-1	762.64	729.7	-4.51
Sp-2	760.11	733.51	-3.62

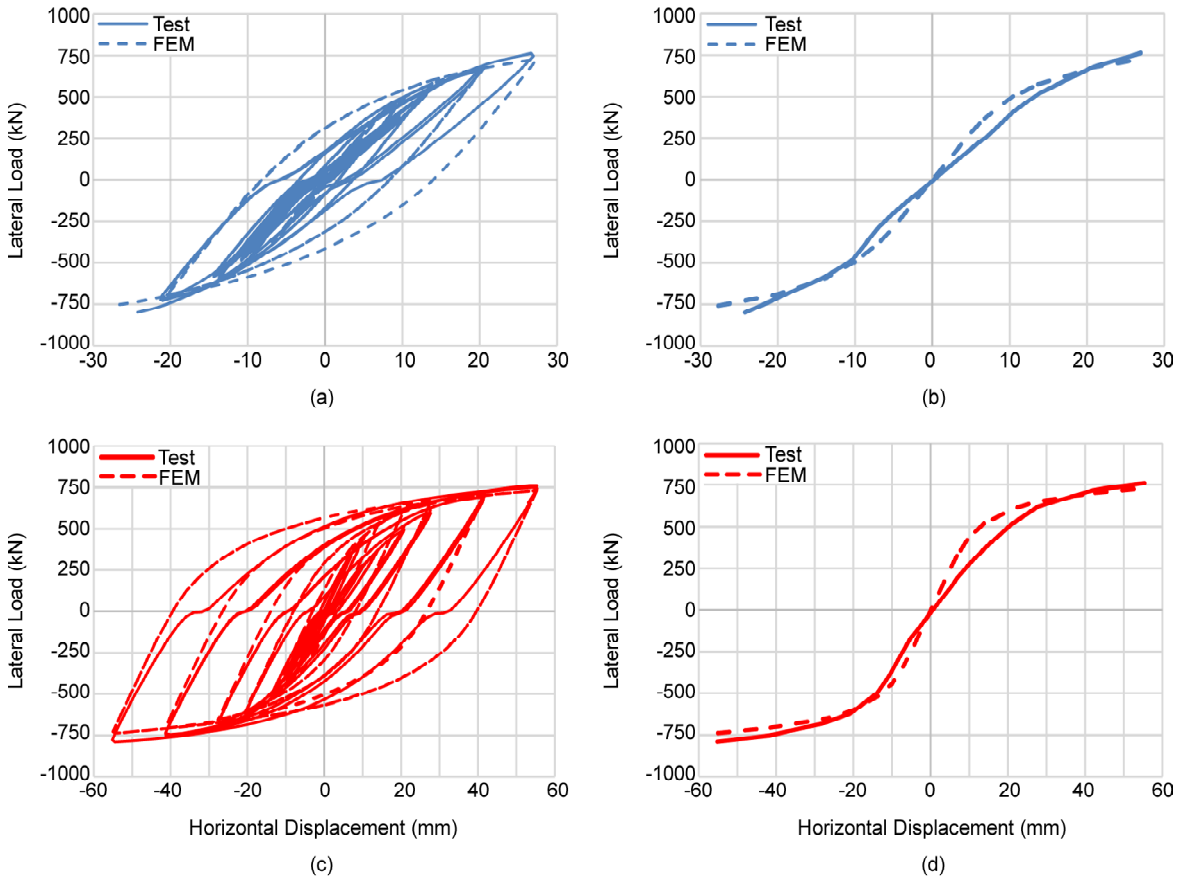

Figure 19. Force-displacement hysteretic curves and back-bone curves: (a) Force-displacement hysteretic curve of Sp-1; (b) Pushover curve of Sp-1; (c) Force-displacement hysteretic curve of Sp-2; (d) Pushover curve of Sp-2.

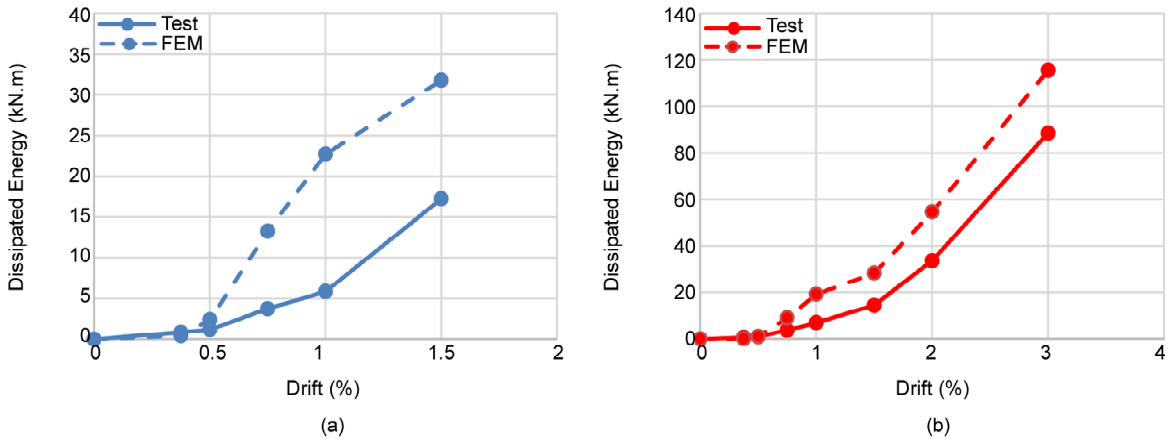

Figure 20. Comparison of FE hysteretic analysis with test results: (a) Sp-1; (b) Sp-2.

Table 6. Height- to- thickness ratio and web panel thickness.

Height-to-Thickness Ratio (λ)	100	150	200	250	300
Thickness t (mm)	7.3	4.87	3.65	2.92	2.43

Table 7. Dissipated energy (kN.m).

Opening Ratio	0	0.2	0.3	0.4	0	0	0	0	0
λ	200	200	200	200	100	150	200	250	300
Dissipated Energy (E) (kN.m)	1622.35	1184.44	1026.19	856.19	2118.8	1829.28	1622.35	1468.25	1353.91
E, rel. (kN.m)/(kN.m)	1.00	0.73	0.63	0.53	1.00	0.86	0.76	0.69	0.64

30% more than that of obtained in test result. The total amount of cumulative dissipated energy in the FE results in Sp-1 and Sp-2 specimens was 70.59 kN.m and 227.92 kN.m, respectively.

4.2. FE Analysis of Steel Frame System with Mid-Span Shear Panel

The numerical analyzes were then performed to investigate the effect of the ratio between opening area to the area of the shear panel (opening ratio) and the ratio of the height of the panel to the thickness of the infill plate (slenderness ratio λ) on the hysteretic behavior of the system. In all the investigated FE models, the dimensional characteristics of the frame, secondary column profiles, maximum shear panel stiffener distance and material properties were considered similar to those of Sp-1 and Sp-2 specimens. As the number of openings changed, the opening ratio changed. By varying the thickness of the web plate of shear panel, the parameter λ changed from 100 to 300. The ratio of shear panel height to web plate thickness is presented in Table (6).

FE models were developed and analyzed. Figure (21) shows the hysteretic load-deformation curves for some models. As it can be seen, the hysteretic curves of FE models are stable and spindle-shaped. By decreasing the slenderness ratio of the infill plate and the opening ratio, the area under the curves increases and thus, the amount of dissipated energy is increased.

Figure (22) shows the dissipated energy versus drift ratio in the two groups of models. In all models, the amount of energy dissipation increases with increasing drift ratio. It is also observed that the amount of dissipated energy decreases with the increase of the opening ratio and the slenderness ratio.

Table (7) presents the total cumulative dissipated energy for the two groups of models (models with slenderness ratio of 200 and models with no openings). For example, in the group of models with slenderness ratio of 200, the dissipated energy in the model with the opening ratio of 0.2, 0.3, and 0.4 is about 27%, 37%, and 47% less than that of the model with no opening, respectively. Moreover, in the models with no opening, by increasing the

slenderness ratio from 100 to 150, 200, 250, and 300, the dissipated energy decreased by 14%, 24%, 31% and 36%, respectively.

Table (8) summarizes the shear capacity of the models. As it can be seen, increasing the opening ratio and also slenderness ratio of the infill plate in the shear panel, decreases the shear capacity of the system. For example, in models with slenderness

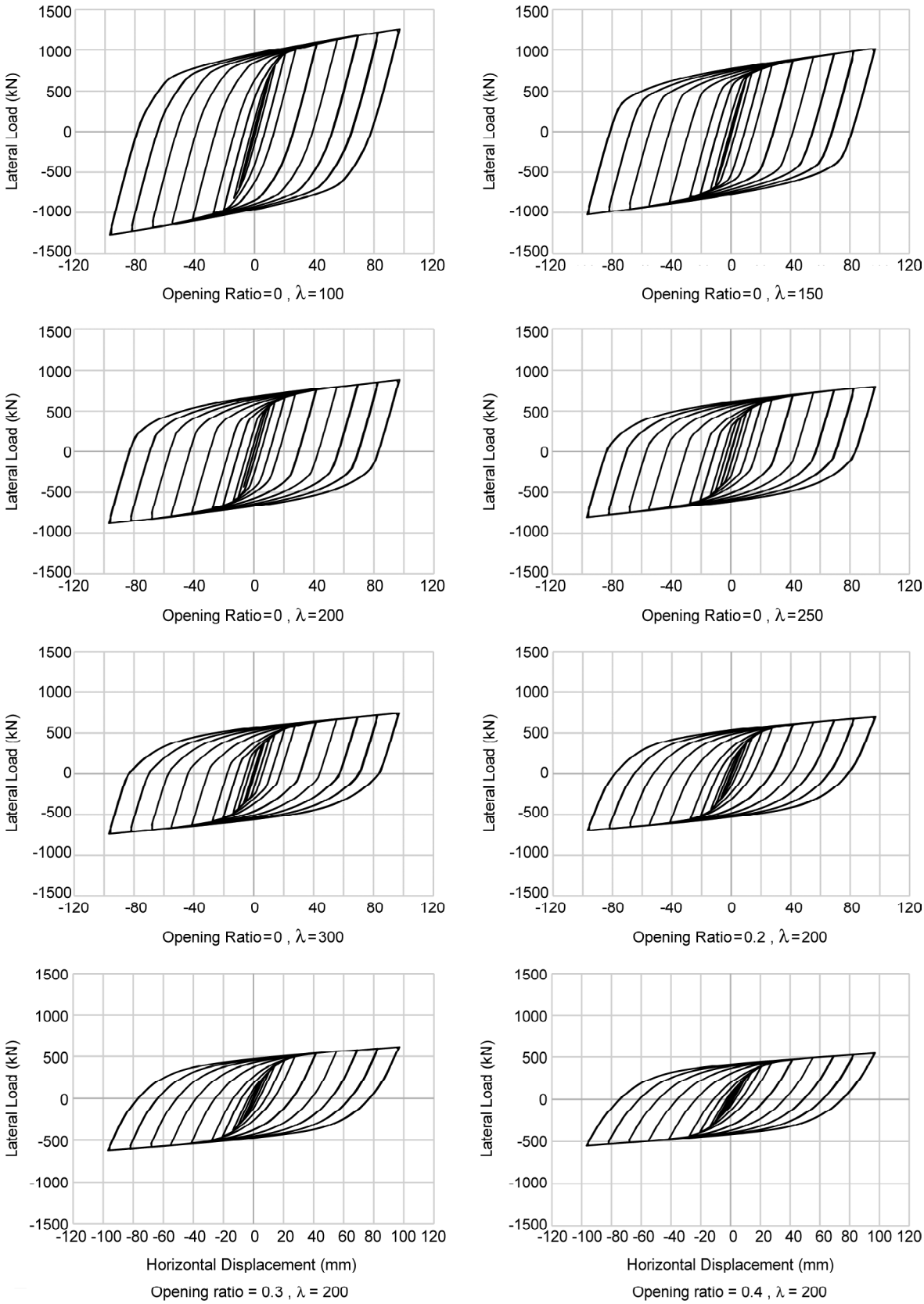

Figure 21. Hysteretic curves of FE models.

ratio of 200, the maximum strength in models with opening ratios of 0.2, 0.3, and 0.4 is about 21%, 30%, and 38% lower than that of the model without opening, respectively. Moreover, in models without opening, by increasing the slenderness ratio from 100 to 150, 200, 250 and 300, the maximum strength decreased by 19%, 30%, 36%, and 41%, respectively.

Figure (23) shows the secant stiffness based on drift ratio in two groups of models. In all models, the secant stiffness decreased by increasing the drift ratio. The reduction rate was more rapid in models with lower opening ratio. Increasing the slenderness ratio did not have a significant effect on the reduction rate of secant stiffness.

5. Conclusion

This paper presents numerical and experimental studies on pinned steel frame system with a middle span shear panel in order to investigate the cyclic behavior of the system and the effect of opening ratio on its behavior. The presence of boxes in the system is considered to separate the gravity and lateral load resisting systems and to achieve a

Table 8. Max. strength (kN).

	Opening Ratio = 0	Opening Ratio = 0.2	Opening Ratio = 0.3	Opening Ratio = 0.4
λ =100	1255.14	901.86	777.85	660.90
λ =150	1019.38	770.92	675.32	585.84
λ =200	882.19	696.22	617.80	546.16
λ =250	797.59	646.9	580.75	521.84
λ =300	739.9	612.02	554.26	503.85

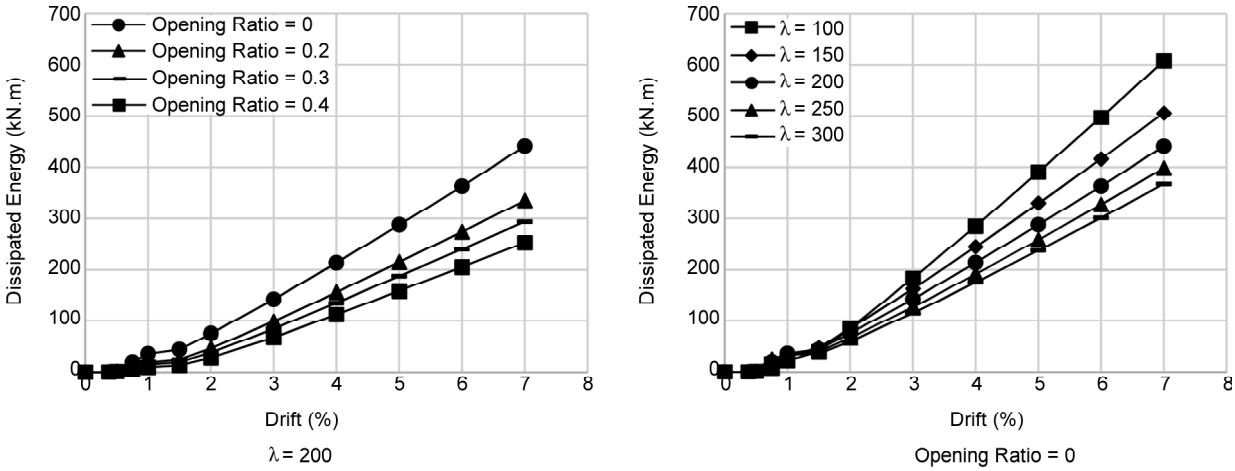

Figure 22. Dissipated energy in each drift ratio.

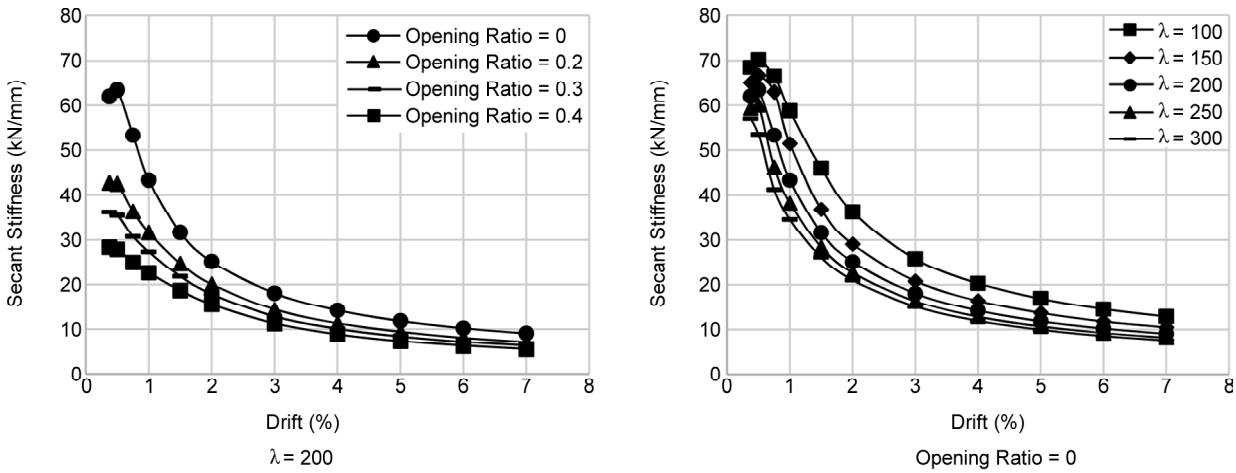

Figure 23. Secant stiffness in each drift ratio.

repairable system. On the other hand, as the shear panel length decreases, its behavior becomes closer to that of a shear link beam. The tests were performed on two specimens with a scale of 1:2 and the only difference between the two specimens was the presence of opening in the second specimen. FE analysis was performed on 20 models to investigate the effect of slenderness ratio of infill plate and opening ratio on the behavior of system. The most important results of this research can be summarized as follows:

- Test results on Sp-1 and Sp-2 specimens showed good energy dissipation and stable hysteretic curves.
- The shape of the hysteretic curves of the specimens were spindle shaped and the pinching phenomenon was not observed.
- In the Sp-1 and Sp-2 specimens, the experiment continued until cycle 25 (2% drift ratio) and cycle 29 (4% drift ratio), respectively. Experimental results on the two specimens showed that the presence of openings in the system reduces shear strength, energy dissipation and elastic stiffness.
- The presence of opening with a surface ratio of 20% reduced the initial stiffness of the system by about 26%.
- The ratio of maximum shear strength in cycle 25 (2% drift ratio), in Sp-1 specimen to Sp-2 specimen was 1.3.
- In both experimental specimens, the secant stiffness decreased with increasing drift ratio. The reduction was more rapid in the specimen with opening than in the other specimen. Secant stiffness was higher in the specimen without opening than that in the other specimen.
- The amount of energy loss in the specimen with no opening (Sp-1) was 1.2 times than that of the specimen with opening (Sp-2). Moreover, the ratio of cumulative dissipated energy at 1.5% drift ratio, in Sp-1 to Sp-2 was 1.08.
- The measured strains were in good agreement with the observed failure modes. The results of the strain gauges showed that in both tests, after the drift ratio of 0.5%, the infill plate yielded and then, the secondary columns were yielded during the loading progress.
- In both tested specimens, the elastic stiffness obtained from the test results was less than that of the FE analysis results. The difference may be due to the slippage between the loading beam and the frame, as well as localized imperfections in the system during the test.
- The shear capacity obtained from numerical modeling was in good agreement with the test results. In the two specimens Sp-1 and Sp-2, the difference between the shear capacity obtained from the experimental and numerical results was less than 5%.
- In the two studied specimens Sp-1 and Sp-2, the amount of energy loss from FE analysis was greater than the value obtained from the experimental results. For example, at 1.5% drift ratio, the amount of dissipated energy from the FE analysis results in the Sp-1 and Sp-2 specimens was 1.8 and 1.9 times that of the experimental results, respectively.
- The results of FE analysis showed that by in creasing the opening ratio, the amount of dissipated energy and the maximum strength decreased. For example, in models with slenderness ratio of 200, the dissipated energy and maximum strength in the model with an opening ratio of 0.4 were about 47% and 38% less than that of the model without opening, respectively. Furthermore, in the models without opening, with increasing of slenderness ratio from 100 to 300, the amount of dissipated energy and maximum strength decreased by 36% and 41%, respectively.
- Comparison of FE analysis showed that when the drift ratio is increased, the secant stiffness decreases. The reduction was more rapid in specimens with lower opening ratio.

Acknowledgment

This work was supported by the International Institute of Earthquake Engineering and Seismology (IIEES), under Project ID 678. The authors would like to gratefully thank the IIEES for supporting this research. The authors appreciate the support and accept the full responsibility for the work and conclusions presented.

References

1. Sabouri-Ghomi, S., Roberts, T. (1992) Nonlinear dynamic analysis of steel plate shear walls including shear and bending deformations.

Engineering Structures, **14**(5), 309-17.

2. Elgaaly, M., Caccese, V., and Du, C. (1993) Postbuckling behavior of steel-plate shear walls under cyclic loads. *Journal of Structural Engineering*, **119**(2), 588-605.

3. Driver, R.G., Kulak, G.L., Elwi, A.E., and Kennedy, D.L. (1998) FE and simplified models of steel plate shear wall. *Journal of Structural Engineering*, **124**(2), 121-130.

4. Driver, R.G., Kulak, G.L., Kennedy, D.L., Elwi, A.E. (1998) Cyclic test of four-story steel plate shear wall. *Journal of Structural Engineering*, **124**(2), 112-120.

5. Astaneh-Asl, A. (2001) *Seismic Behavior and Design of Steel Shear Walls*. Steel TIPS Report.

6. Sabouri-Ghomi, S., Ventura, C.E., and Kharrazi, M.H. (2005) Shear analysis and design of ductile steel plate walls. *Journal of Structural Engineering*, **131**(6), 878-89.

7. Shekastehband, B., Azaraxsh, A., Showkati, H., and Pavir, A. (2017) Behavior of semi-supported steel shear walls: Experimental and numerical simulations. *Engineering Structures*, **135**, 161-176.

8. Berman, J.W. and Bruneau, M. (2005) Experimental investigation of light-gauge steel plate shear walls. *Journal of Structural Engineering*, **131**(2), 259-67.

9. Vian, D., Bruneau, M., Tsai, K-C., and Lin, Y-C. (2009) Special perforated steel plate shear walls with reduced beam section anchor beams. I: Ex perimental investigation. *Journal of Structural Engineering*, **135**(3), 211-20.

10. Purba, R. and Bruneau, M. (2009) Finite-element investigation and design recommendations for perforated steel plate shear walls. *Journal of Structural Engineering*, **135**(11), 1367-1376.

11. Driver, R.G., Grondin, G.Y., Behbahanifard, M.R., and Hussain, M.A. (2001) Recent developments and future directions in steel plate shear wall research. *NASCC Proceedings*.

12. Guo, L., Rong, Q., Ma, X., and Zhang, S. (2011) Behavior of steel plate shear wall connected to frame beams only. *International Journal of Steel Structures*, **11**(4), 467-479.

13. Vatansever, C. and Yardimci, N. (2011) Experimental investigation of thin steel plate shear walls with different infill-to-boundary frame connections. *Steel and Composite Structures*, **11**(3), 251-71.

14. Jahanpour, A., Jonsson, J., and Moharrami, H. (2012) Seismic behavior of semi-supported steel shear walls. *Journal of Constructional Steel Research*, **74**, 118-33.

15. Clayton, P.M., Berman, J.W., and Lowes, L.N. (2015) Seismic performance of self-centering steel plate shear walls with beam-only-connected web plates. *Journal of Constructional Steel Research*, **106**, 198-208.

16. Shekastehband, B., Azaraxsh, A., and Showkati, H. (2018) Experimental seismic study on shear walls with fully-connected and beam-only-connected web plates. *Journal of Constructional Steel Research*, **141**, 204-15.

17. AISC (2010) *Seismic Provisions for Structural Steel Buildings AISC 341-10*. Chicago: American Institute of Steel Construction.

18. ASTM (2006) *Standard Test Methods and Definitions for Mechanical Testing of Steel Products. ASTM A370*. American Society for Testing and Materials (ASTM). West Conshohocken, USA.

19. Clark, P., Frank, K., Krawinkler, H., and Shaw, R. (1997) *Protocol for Fabrication, Inspection, Testing, and Documentation of Beam-Column Connection Tests and Other Experimental Specimens*. SAC Steel Project Background Document (Report No. SAC/BD-97/02).

20. Simulia (2013) *ABAQUS Version 6.13-4 Documentation*.